An Experimental Investigation of Leading Edge Vortices and Passage to Stall of Nonslender Delta Wings

Michael V. Ol
Michael.Ol@wpafb.af.mil
AFRL/VAAA, BLDG. 45, 2130 8th St.
Wright-Patterson AFB, OH 45433-7542, USA
Air Vehicles Directorate, Air Force Research Laboratory, USA

Abstract

This paper describes an experimental investigation of the structure and decay of the leading edge vortices (LEVs) produced by a nonslender delta wing. The work was conducted in a water tunnel facility at the California Institute of Technology, and was sponsored by the Air Force Research Laboratory (AFRL). Stereoscopic digital particle image velocimetry was used to obtain three-component velocity data in planar slices across the flowfield above the wing leeward surface. These measurements were motivated by flow visualization by dye injection.

Delta wings of 50° and 65° leading edge sweep at Reynolds numbers of 8000 and 14000, respectively, were studied. For both wings, stable primary LEVs were observed over the entire planform for 5° angle of attack and below. For the 50° wing, the secondary LEVs were found to decay more abruptly and at lower angle of attack than the primary LEVs, all but disappearing by 10° angle of attack. This suggests a possible predictive criterion for breakdown of the primary vortices, at least at low Reynolds number. The entire vortex system undergoes large-scale instabilities in the 12°-20° angle of attack range. The leading edge shear layer, however, remains in an organized rolled-up state in this angle of attack range. By 20°, the flow over the leeward side of the wing is completely stalled.

Introduction

The static stall behavior of high aspect ratio (e.g., rectangular, straight-tapered, or moderately swept) wings is a classical problem. Likewise, for slender delta wings the organized separated flow and the leading edge vortex (LEV) breakdown has also been extensively investigated, especially for steady state conditions. However, the transitional case – that of the delta wing of relatively high aspect ratio – is presently of some ambiguity. This paper considers the case of a sharp-edged delta wing of 50° leading edge sweep (aspect ratio 3.36). The 50° wing is compared to a 65° wing (aspect ratio 1.87) of similar geometry. Reynolds number based on root chord was 8000 for the 50° wing and 14,000 for the 65° wing.

The LEVs of slender, sharp-edged delta wings are subject to decay at high angles of attack by the well-known (though not entirely understood) mechanism of vortex breakdown. Typically, with increasing angle of attack, it is the upstream progression of breakdown toward the wing apex that results in a stall-type situation. Here, one speaks of stall not in the "airfoil sense" of the mere presence of large-scale separated flow, but in the sense that organized, well-defined separation associated with the pre-stall condition has given way to a disorganized flow of low aerodynamic efficiency[1]. The process of passage toward stall can occur in various forms and to various extents of unsteadiness[2], but because the angle of attack slender wing stall is quite high, interaction of the primary LEVs and near-surface phenomena, such as the secondary vortices, is limited[3].

Paper presented at the RTO AVT Symposium on "Advanced Flow Management: Part A – Vortex Flows and High Angle of Attack for Military Vehicles", held in Loen, Norway, 7-11 May 2001, and published in RTO-MP-069(I).

Report Documentation Page

Form Approved
OMB No. 0704-0188

1. REPORT DATE	2. REPORT TYPE	3. DATES COVERED
00 MAR 2003	**N/A**	**-**

4. TITLE AND SUBTITLE	5a. CONTRACT NUMBER
An Experimental Investigation of Leading Edge Vortices and Passage to Stall of Nonslender Delta Wings	5b. GRANT NUMBER
	5c. PROGRAM ELEMENT NUMBER
6. AUTHOR(S)	5d. PROJECT NUMBER
	5e. TASK NUMBER
	5f. WORK UNIT NUMBER
7. PERFORMING ORGANIZATION NAME(S) AND ADDRESS(ES) **NATO, Research and Technology Organisation, BP 25, 7 rue Ancelle, F-92201 Neuilly-Sur-Seine Cedex, France**	8. PERFORMING ORGANIZATION REPORT NUMBER
9. SPONSORING/MONITORING AGENCY NAME(S) AND ADDRESS(ES)	10. SPONSOR/MONITOR'S ACRONYM(S)
	11. SPONSOR/MONITOR'S REPORT NUMBER(S)

12. DISTRIBUTION/AVAILABILITY STATEMENT
Approved for public release, distribution unlimited

13. SUPPLEMENTARY NOTES
Also see: ADM001490, The original document contains color images.

14. ABSTRACT

15. SUBJECT TERMS

16. SECURITY CLASSIFICATION OF:			17. LIMITATION OF ABSTRACT	18. NUMBER OF PAGES	19a. NAME OF RESPONSIBLE PERSON
a. REPORT	b. ABSTRACT	c. THIS PAGE			
unclassified	**unclassified**	**unclassified**	**UU**	**16**	

For a 60° wing, Shih and Ding[3] have identified the importance of the secondary LEV in affecting the primary LEV, and in particular, in interacting with identifiable vortical structures within the leading edge shear layer. Indeed, there has been considerable recent interest in the role of such structures. The present study extends these results to the 50° wing. Broadly speaking, the higher the aspect ratio (or interchangeably, the lower the leading edge sweep angle), the lower the angle of attack identifiable with the onset of stall. At the low incidence angles considered in the present study, the LEVs are close to the wing surface, and vortex breakdown regions interact strongly with flow near the leeward surface. Meanwhile, one qualitative effect of low Reynolds is to broaden the "core" region of the primary LEVs to the point where they extend nearly all the way to the wing leeward surface, as viewed in crossflow planes. The attention to low Reynolds number is motivated by the long list of delta wing experiments conducted in water tunnels, and the issue of how such data scale to the higher Reynolds numbers associated with flight conditions; see, for example, Erickson[4], Poisson-Quinton and Werle[5], and Thompson[6].

For the 50° wing, the passage toward stall is appreciably different than for slender wings. For the conditions of the present experiments, at angles of attack below 12°, the 50° wing developed strong primary and unusually strong secondary LEVs, with breakdown near the trailing edge. This is rather different from some earlier results[7] for this sweep angle. Classical results, mostly at higher Reynolds number, also suggest that wings of such low sweep do not generate appreciable LEVs (reference [8] for example).

Despite the low angle of attack persistence of coherent vortical flow, evidence of stall-like behavior is already present at around 10° AOA, where the secondary LEVs are markedly weakened. Between 12° and 20° AOA, the primary LEV undergoes large-scale unsteadiness manifested in quasi-periodic back and forth streamwise movement of breakdown, reversal and outboard redirection of flow adjacent to the leeward surface, and reformation of the LEV. The wing "stalls" by 20 degrees angle of attack, with a separated "bubble" enveloping the leeward surface. Flow visualization reveals that this region is bounded from the ambient flow by shear layer that itself displays Kelvin-Helmholtz waviness.

The principal experimental technique used in the present experiment is that of stereoscopic digital particle image velocimetry ("SPIV"). All three components of velocity are obtained over a sequence of planar domains, tracking the trajectory of the primary LEV core. An "instantaneous" snapshot of the flowfield is obtained, in contrast with the time-averaged data resulting from traverses of a single-point diagnostic tool such as LDV, hot wires, etc. SPIV is especially useful in situations with appreciable unsteadiness, such as in the 10°-20° angle of attack range for the 50° wing.

Experimental methods

All data were taken in a low-speed free-surface water tunnel built in conjunction with the present experiment. The facility has a 45cm by 60cm by 240cm test section and a flow speed range of 3.2-50cm/s, with nominal turbulence intensity of about 1%. Details of the facility are given in [9].

The two wing models used in this experiment were made of 1/8" Plexiglas , with a common trailing edge span of 180mm, 30° windward-side bevels and flat leeward surface. The models and their mounting arrangement are shown in Figure 1. The arrangement of the SPIV interrogation planes – that is, those domains in the flowfield over which the SPIV data were taken – are shown schematically in the planform view in Figure 2. The domain of the SPIV data was biased toward the wing apex in an effort to capture the flowfield in succeeding downstream stations with reasonable resolution without changing the optical settings of the laboratory setup. Moreover, it was expected that large qualitative changes in the LEV behavior would also be captured in this region, without having to sweep over the entire wing planform.

A "rotational" arrangement of SPIV[10] was adapted to the environment of a water tunnel; details are also given in [9]. Video-based image sequences were taken in planar cuts normal to the free

stream, passing through the wing model and in particular, focusing on the starboard primary and secondary LEV region.

Flow visualization was conducted by injecting dye (mixture of food coloring and water) via a 0.5mm diameter probe into the nominal region about the windward stagnation point just after of the model apex. This probe can be seen as a thick dark line in the following visualization images. Location of the probe near to model line of symmetry resulted in dye entrainment into both port and starboard primary LEVs. A biasing of the probe location off-center resulted in most of the dye convecting along that wing panel's primary [and where applicable, secondary] LEV. Side-view and planform-view images were taken simultaneously by making use of the video and software techniques as for the SPIV setup.

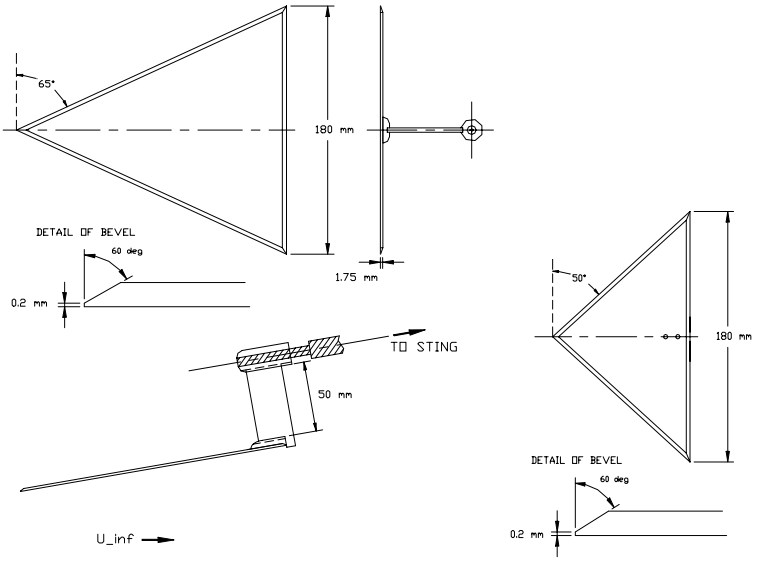

Figure 1. 65° and 50° wing models, with mounting arrangement

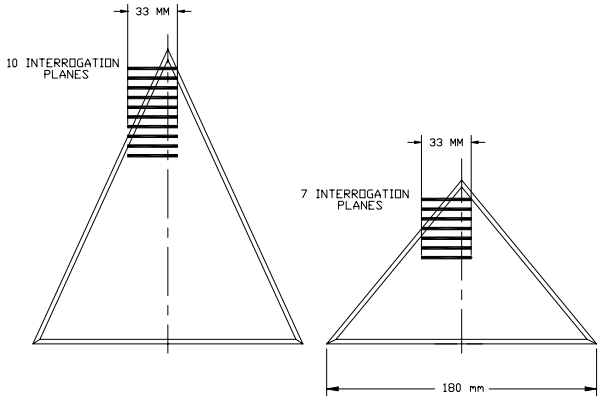

Figure 2. Arrangement of PIV interrogation planes

Results

Results for flow visualization are discussed first, with emphasis on the 50° wing. These data are then used to motivate the SPIV velocity data.

Flow Visualization

We consider three different situations: symmetric port and starboard primary LEVs; dye injection biased to reveal primary and secondary LEVs on one wing panel; and bulk unsteadiness in the entire vortex system.

Stable symmetric primary LEVs

Figure 3 shows essentially symmetric port and starboard primary LEVs for both wings at α = 5°. For the 50° wing, loss of a steady continuous dye streak, akin to vortex breakdown, is observed aft of the trailing edge. For the 65° wing, a similar phenomenon is also observed, though not for approximately one root chord behind the trailing edge. At this low angle of attack, the LEV were weak but definitely visible.

Progressing to α = 10° (Figure 4) shows straighter and more vigorous dye streaks, indicative of stronger primary LEVs. The 65° wing is qualitatively unchanged. However, the 50° wing exhibits symmetric classical breakdown at approximately x/c = 0.7. Flow inside and downstream of the breakdown regions is of course unsteady, but flow upstream of breakdown is steady, as is the position of the leading edges of the breakdown regions.

By α = 20° (Figure 5), breakdown has crossed the trailing edge of the 65° wing.

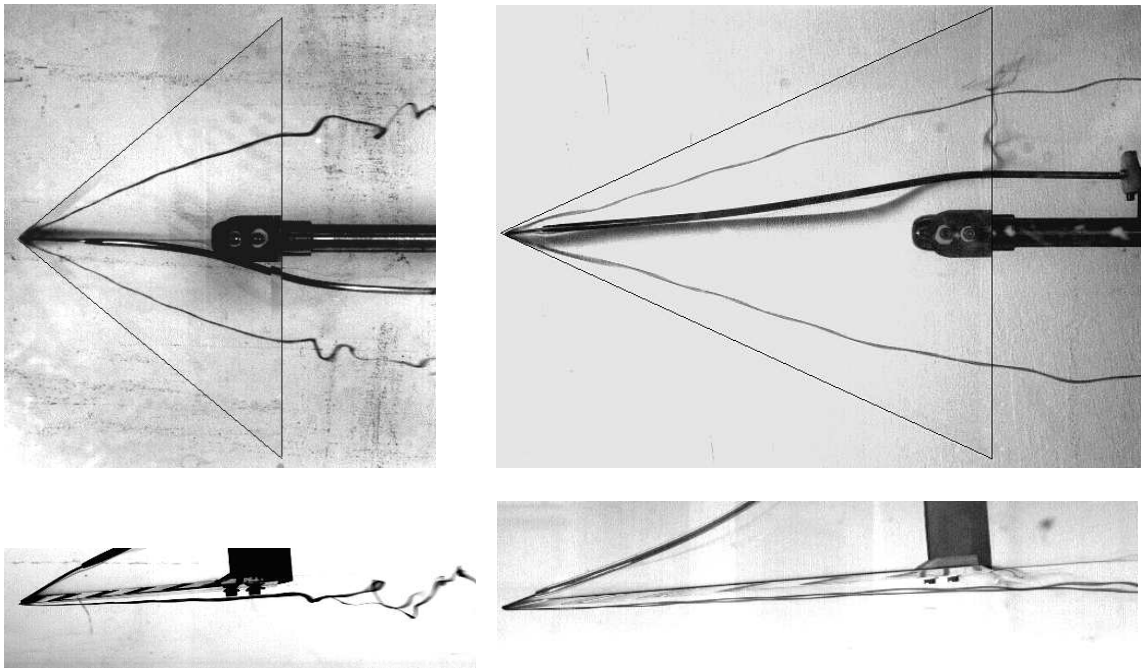

Figure 3. Dye streaks following primary LEVs for 50° and 65° wings, at α = 5°; planform and side views.

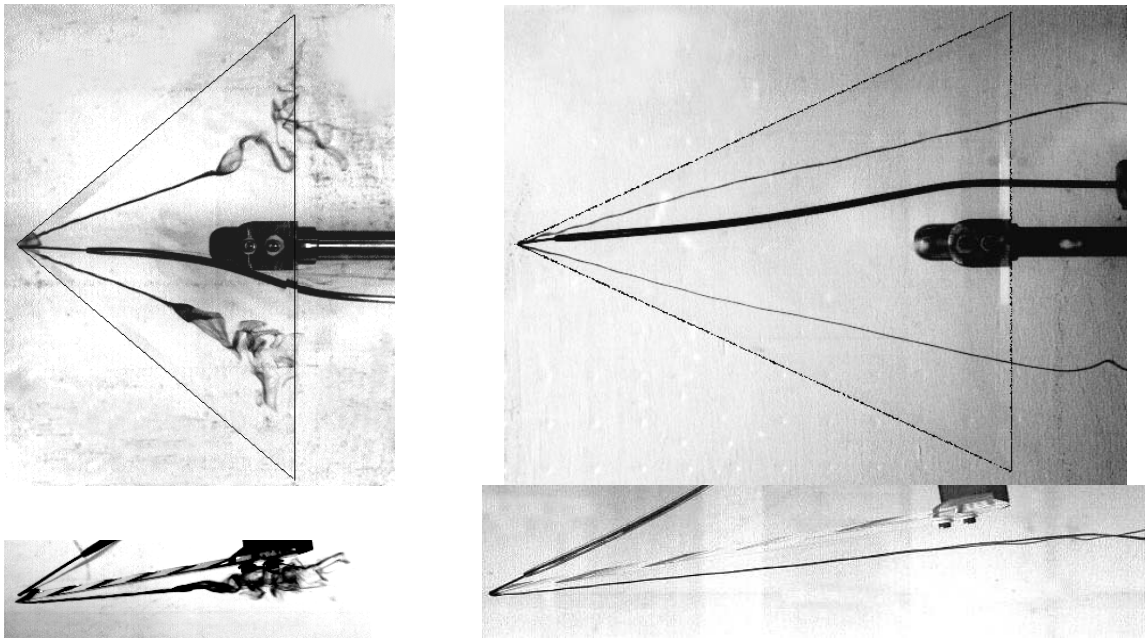

Figure 4. Dye streaks following primary LEVs for 50° and 65° wings, at α = 10°; planform and side views.

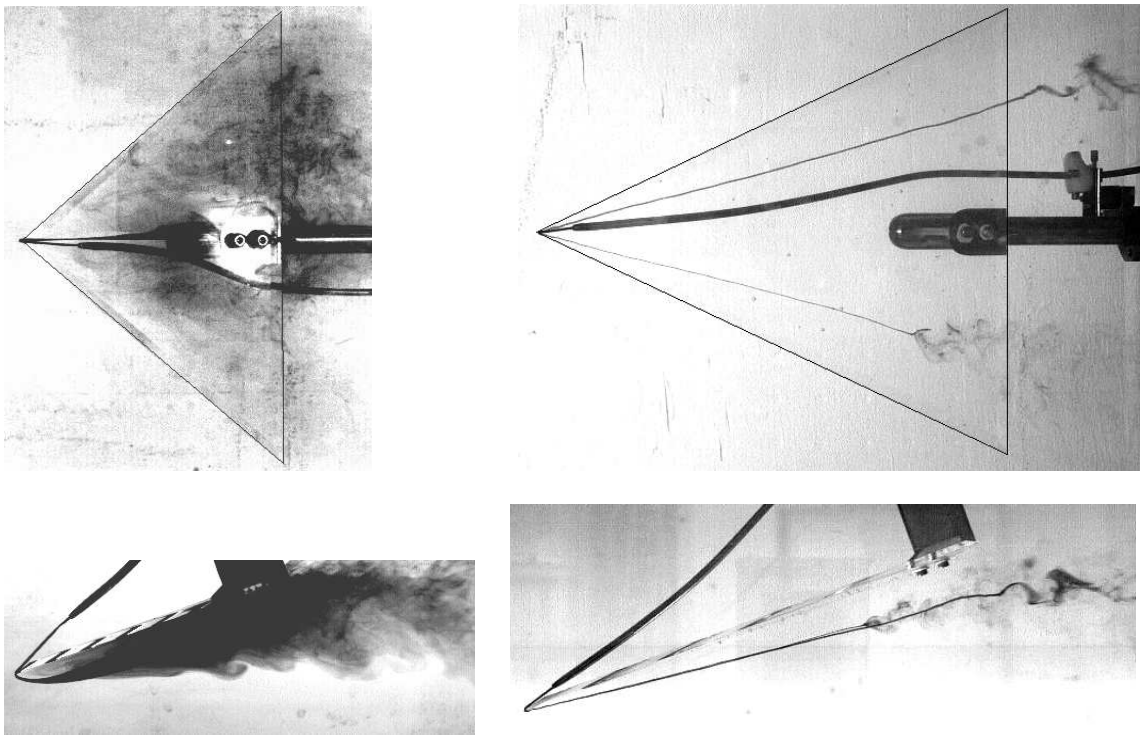

Figure 5. Dye streaks following primary LEVs for 50° and 65° wings, at α = 20°; planform and side views. 50° wing is completely stalled.

Secondary Vortices for the 50° wing

In Figure 6, the starboard-side primary and secondary LEV dye streaks are shown. In going from 5° to 7.5° to 10° angle of attack, the secondary LEV is seen to undergo a breakdown-like behavior. At the lowest angle of attack, its dye streak is coherent all the way to the trailing edge. At the intermediate angle, the dye streak widens and the dye flow rate decelerates at approximately the midchord. At 10° angle of attack, the secondary LEV dye streak is very faint.

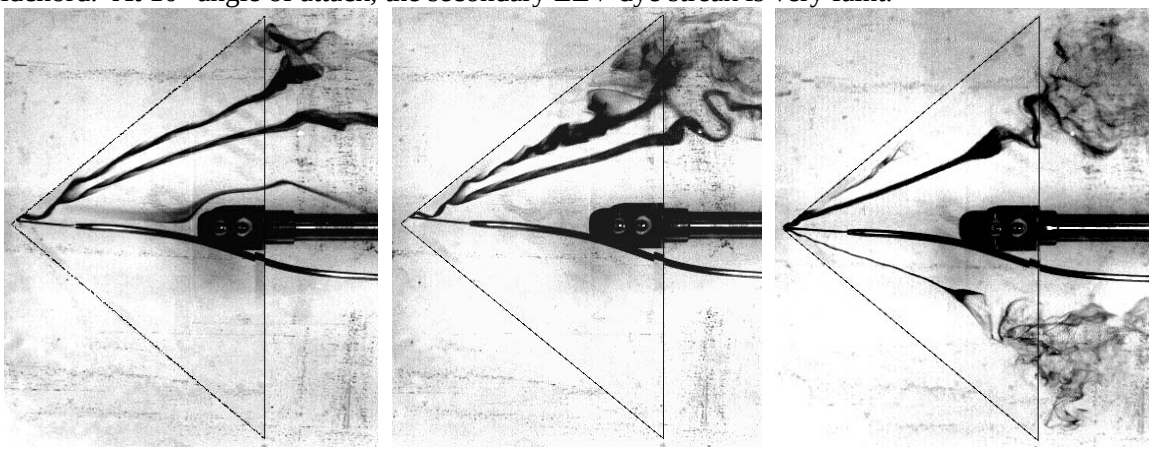

Figure 6. Evolution of secondary LEV: α = 5°, 7.5°, and 10°, 50° wing

Unsteadiness of the 50° wing flowfield

The higher angle of attack cases display marked unsteadiness – that is, there is an apparent exchange of stability between the left and right primary LEVs. Unsteadiness downstream of the breakdown region, and in the vicinity of the VB region itself, has long been known. Here we investigate unsteadiness upstream of VB, with the observation that in the following cases - and only in the following cases – was such flow behavior observed. The 65° wing has no such behavior at the angles of attack under consideration. Of course, at higher angles of attack, there is evidence that even quite slender wings have such LEV unsteadiness upstream of the VB point, en route to the complete flow separation at 90° angle of attack (Ayoub and McLachlan[2]).

Among the angles of attack considered here, appreciable unsteadiness was seen in the range of 12.5°-17.5° for the 50° wing, though some variation in the VB location is already displayed at 10°. At 20°, there was not enough recognizable LEV structure to consider unsteadiness to be relevant, beyond fluctuations in the shear layer bounding the leeward separation region (Figure 5).

In the following, a typical time history for the 12.5° case is illustrated by a series of frame captured from video. Frame spacing in time is nondimensionalized with respect to convective time, defined here as $t^* = c/U_\infty$, which for the 50° wing computes to 1.34 seconds, or ~40 video frames for a typical 30 frame/sec video camera. The series is started from nominal time zero. The question of periodicity in the destruction and reformation of coherent LEVs, or the upstream and downstream procession of the left and right VB, is intriguing but largely unresolved, due in part to the very long data records necessary to capture such a slowly evolving motion. Some qualitative observations are given below. Frame time, *t*, is given in multiples of t^*.

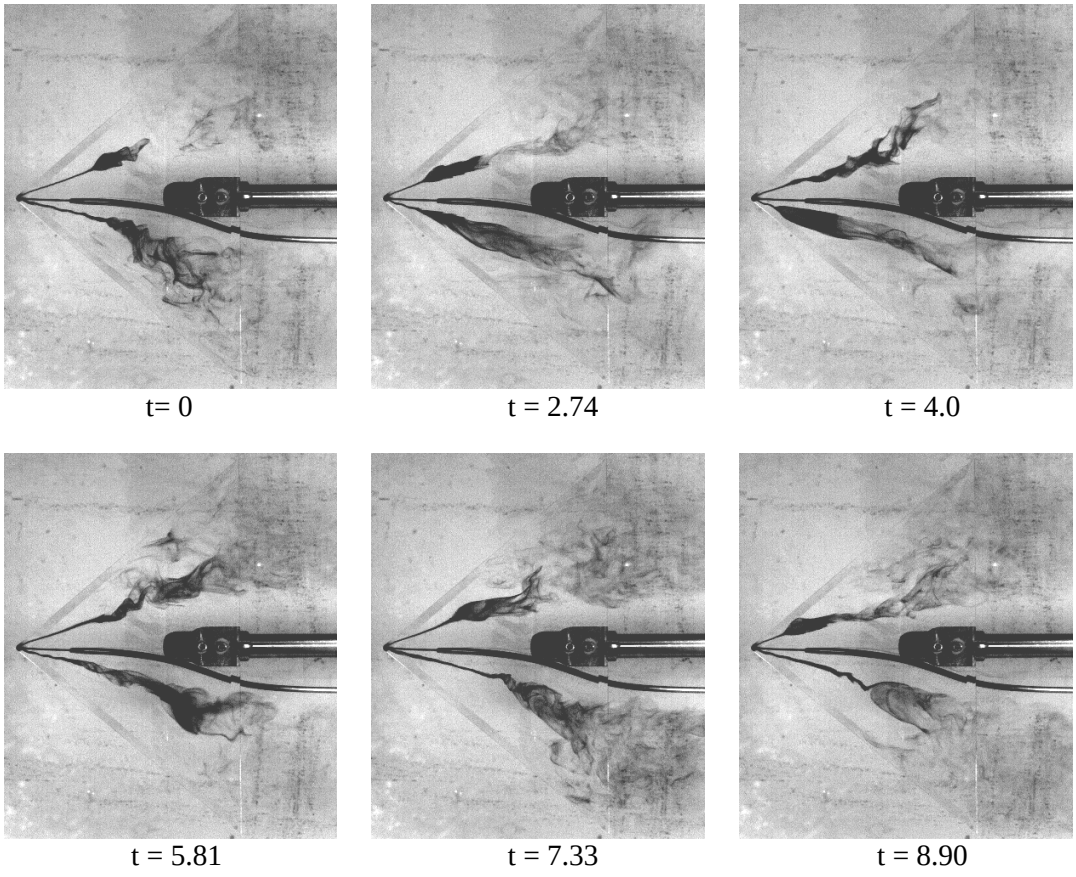

Figure 7. Typical sequence of port and starboard LEV behavior, 50° wing, α = 12.5°

In going from *t = 0* to *t=8.9*, the behavior of the LEVs can be described as follows: a bubble-like VB region on the starboard side forms and moves upstream, while on the port side, an elongated bubble forms by coalescence of a wavy (but not spiral) breakdown structure. By *t = 3*, the port structure overtakes the starboard structure in its upstream movement. The starboard LEV then reforms, dissipating its VB bubble and replacing it with a wavy-type breakdown much further downstream, while the port-side elongated bubble lingers near the apex. By *t=6* the port-side bubble also collapses to a tight vortex core, and the starboard-side VB region again coalesces to a bubble. This bubble then resumes its upstream journey, while the port-side VB region retreats further downstream and takes on a more typical spiral shape.

Streamwise excursions of VB location are by no means unique to delta wings of moderate sweep, though in the case of wings of larger sweep, the excursions are of much lower extent. For example, the flow visualization data of Truneva[11] revealed streamwise VB excursions of about 10% of root chord, for a wing of 60° sweep at a Reynolds number of ~2500.

SPIV velocity data

SPIV velocity vector plots are given below for the 50° (Figure 8) and 65° (Figure 9) wings. In an effort to illustrate three-component vector data from their two-dimensional domain, two views are given. The first is a “streamwise view”, with the free-stream direction normal to the page. The wing centerline is at x/c = 0. The second view is the planform view, edited to show only that portion of the interrogation domain which is at or below the z-cut passing through the primary LEV core. The colorbar legend indicates the total velocity magnitude, normalized by the free stream value.

Images are averages taken over 200 samples, which correspond to 2.8 and 5.0 convective times for the 65° and 50° wings, respectively.

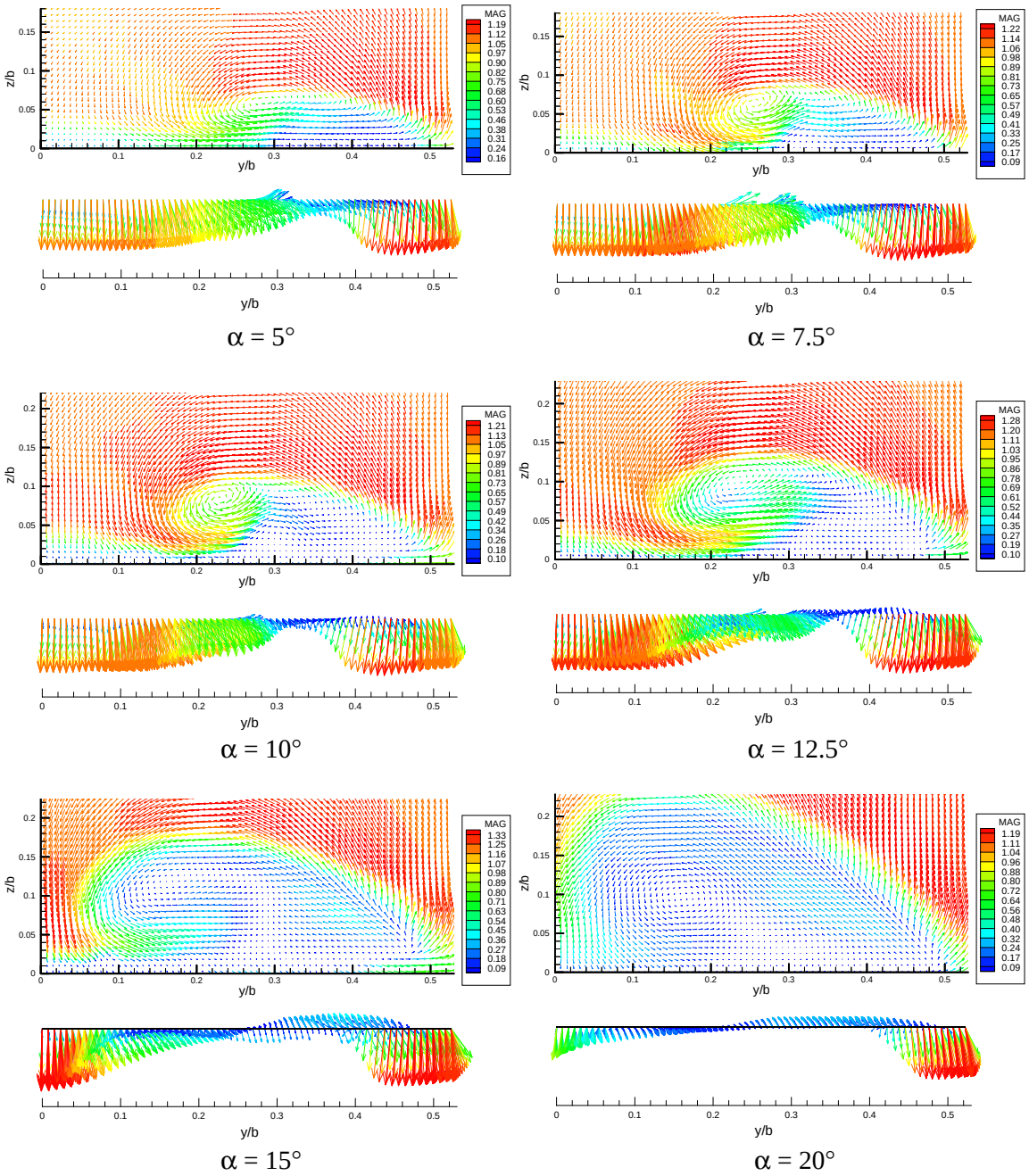

Figure 8. Upstream and planform views of the mean starboard flow pattern, 50° wing; x/c = 0.296; coordinates expressed in fractions of local span.

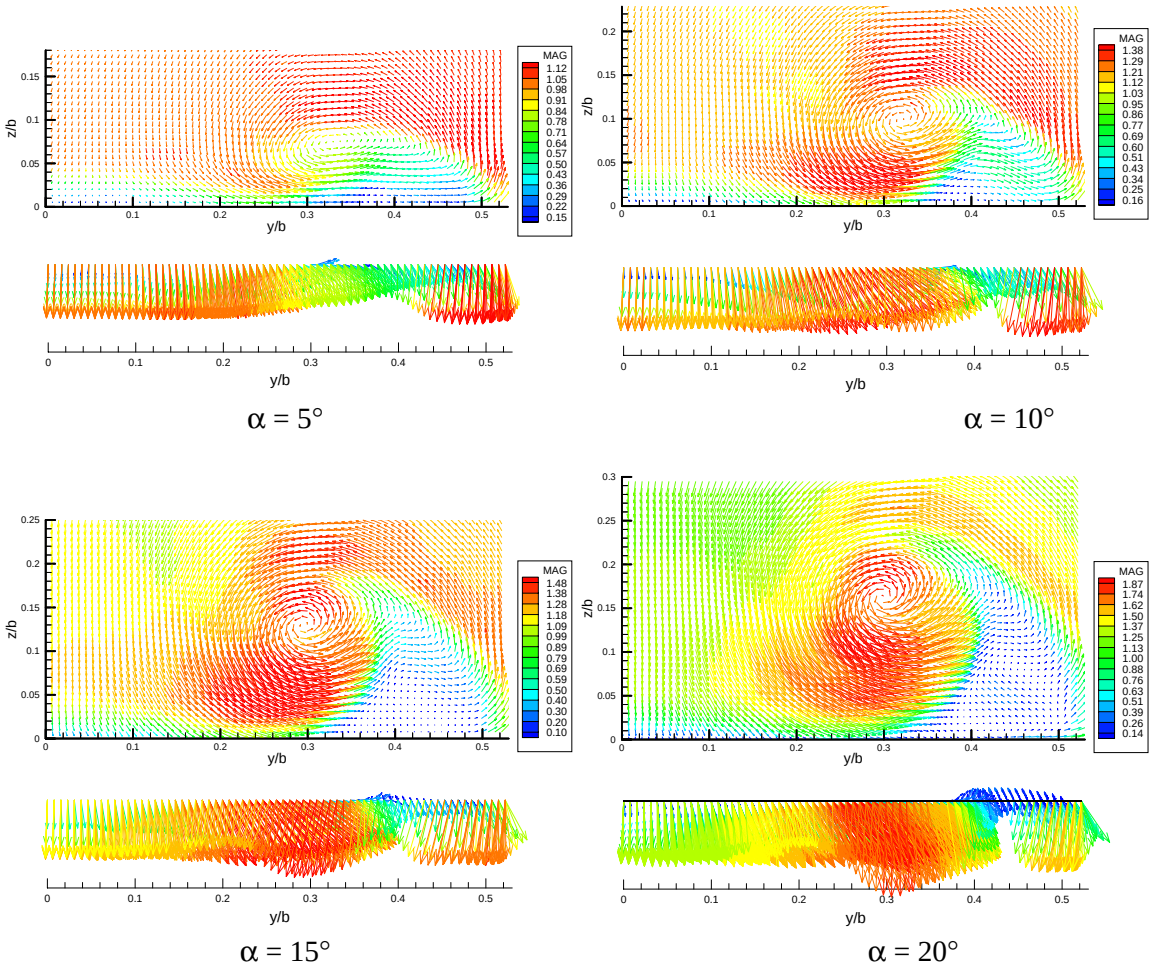

Figure 9. Upstream and planform views of the mean starboard flow pattern, 65° wing; x/c = 0.296; coordinates expressed in fractions of local span.

As expected, the LE shear layer and the LEVs are close to the wing leeward surface at the lowest angle of attack, and move progressively further above the wing with increasing angle of attack. For the 65° wing, axial velocity identifiable with the primary LEV increases with increasing angle of attack, from a value of nearly the same as free stream at 5°, to almost twice that amount at 20°. The latter is consistent with the usual observation the slender delta wing LEVs have high axial core velocity. But the 50°cases exhibit a "wake-like" axial velocity profile usually associated with the post-breakdown leading edge vortex, even when the primary LEV breakdown has clearly not yet cross the interrogation plane in question.

Outboard of the primary LEV, some evidence of a secondary vortex is seen for the lower angle of attack cases. But by 10° angle of attack, the flow velocity magnitude outboard of the primary LEV and inboard of the LE shear layer is nearly zero, indicative of a nearly stagnant flow. This phenomenon was attributed to the effect of low Reynolds number.

Unsteadiness in the 50° wing at moderate angles of attack

In most cases, the averaged velocity data in Figure 8 and Figure 9 differ little from instantaneous data. But that is not the case for the 50° wing at intermediate angles of attack, as evidenced by the flow visualization. Figure 10 illustrates the situation for the 50° wing at α = 15°. Four velocity vector plots represent data taken 1.25 convective times apart. Because true instantaneous data suffer from occasional "outlier" communication (i.e., spurious SPIV data not filtered in post-processing), images were averaged over 5 frames (that is, 0.12 convective times – an interval small enough to retain all but the smallest features of unsteadiness).

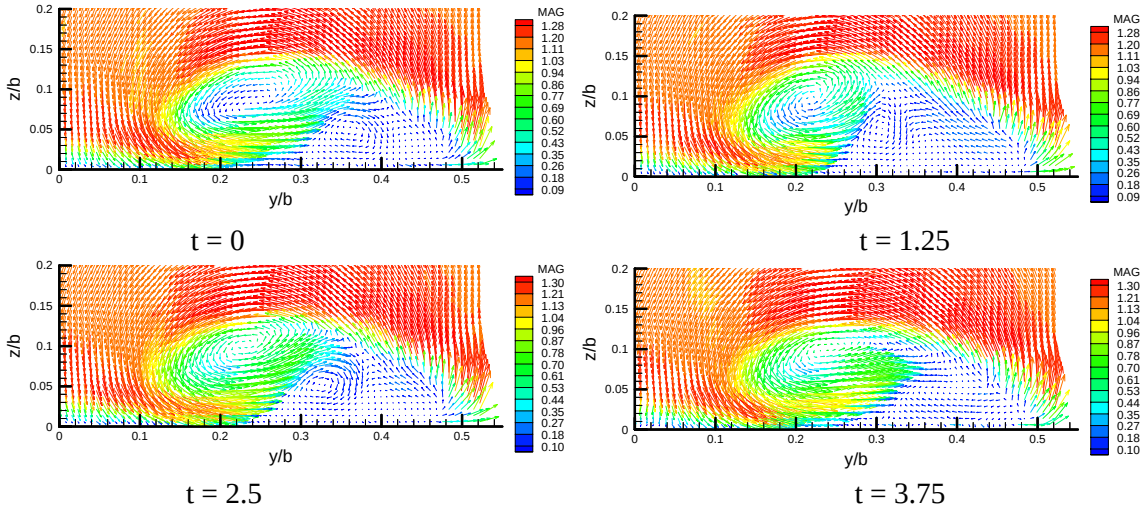

Figure 10. Upstream view of the evolving starboard flow pattern, 50° wing; x/c = 0.296

Appreciable variation in the primary LEV axial velocity can be observed. A weak secondary vortex appears to first occupy its normal position, only to be "swallowed" by the primary LEV. This event is accompanied by an increase in primary LEV axial velocity. Curiously, the flow structure identifiable with this secondary LEV was not expected from the flow visualization data at this angle of attack.

Discussion

With the large data sets generated in these experiments, various derived quantities can be computed from the velocity field. In this paper, two- and three-component vorticity data are considered as examples of possible derived quantities. Others include primary LEV circulation and LEV core trajectories, which are considered further in [9]. We first consider some profiles of the velocity field.

Velocity Profiles

By taking cuts along the appropriate distance above the leeward surface, velocity profiles can be constructed from the vector plots shown in the previous section. Again, one has to contend with the issue of how to represent three-dimensional data. The natural choice is to cut through the primary vortex core. Figure 11 shows these data for the station x/c = 0.296, for both wings and six angles of attack. Data are averaged over 2.8 convective times for the 65° wing, and 5.0 convective times for the 50° wing. The origin is again at the wing centerplane, and the local leading edge is at y = 0.5.

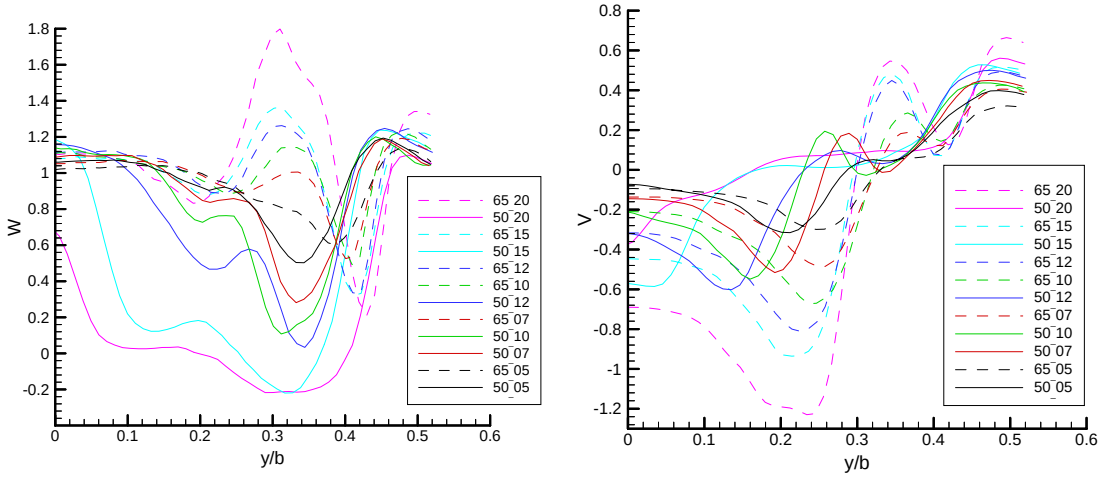

Figure 11. Mean axial and azimuthal velocity profiles, 50° and 65° wings, x/c = 0.296

It is seen from the first half of Figure 11 that the 65° wing has a "jet-like" axial velocity profile in the primary core at angles of attack above 5°. This is modest at small angle of attack, but becomes quite pronounced by 15°. The 50° wing, however, has a "wake-like" behavior at every angle of attack, regardless of whether vortex breakdown is upstream or downstream of the interrogation region. When breakdown has moved upstream of x/c = 0.296, the wake-like profile broadens, expanding further inboard. Complete-stall can be identified with the 20° angle of attack case, with the supposition that de-energized flow characteristic of stall is achieved when the wake-like profiles from the left and right LEVs coalesce at the wing center plane.

In the v-component data, it is seen that there is a peak of positive azimuthal velocity at the wing leading edge, where the shear layer begins its rollup process, for every test case. For the 65° wing, there is the characteristic peak of opposite-signed azimuthal vorticity associated with the primary LEV core. For the 50° wing, the qualitative trend follows that of the 65° wing up to and including 12.5° angle of attack. As the angle of attack increases, data for the 50° and 65° wings progressively diverge. At 15° angle of attack, the velocity profile for the 50° wing changes abruptly, with a loss of velocity peak concomitant with the presence of VB.

For the 65° wing there is a pronounced deficit of both axial and azimuthal velocity component between the primary LEV and the leading edge shear layer. The effect is also present for the 50° wing, albeit attenuated on account of the general lower axial velocity for that wing. This flow retardation is consistent with the results observed by Traub[12] for range for wings of 60° and 70° sweep at Re = 20,000.

Conical flow near the apex

The previous data were presented for one streamwise station, x/c = 0.296. Presently we consider axial velocity profiles at the x/c = 0.118, 0.178, 0.237, and 0.296 stations, for the 50° wing at 12.5° and 15° angles of attack. These are shown in Figure 12, with the common abscissa renormalized with respect to local span.

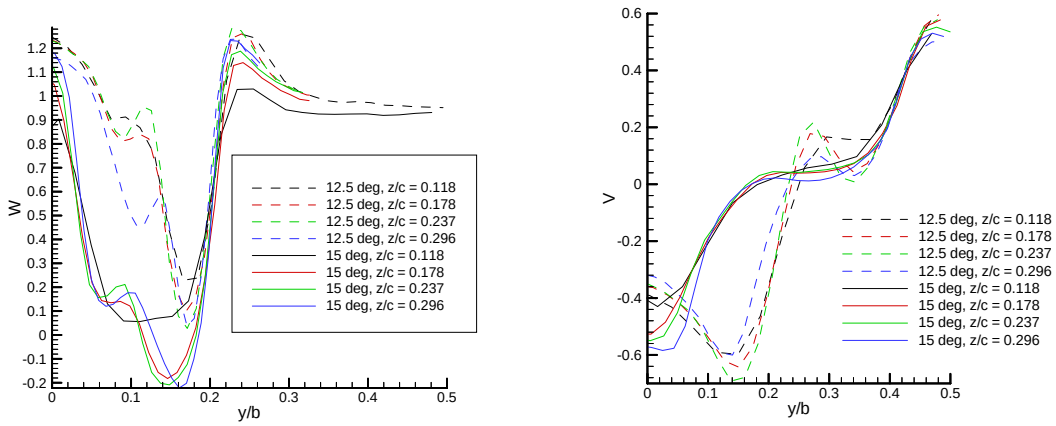

Figure 12. Mean axial and azimuthal velocity profile sweeps, α = 12.5° and 15°

With this rescaling, data for both the 12.5° and 15° AOA become nearly invariant with x/c station. This is strong indication of a conical velocity field. With the exceptions of the x/c = 0.118 15° curve, and the x/c = 0.296 12.5° curve, data in both AOA group almost overlap. In all the curves, the peak in axial velocity occurring near y/b = 0.45 corresponds to the region just outboard of the LE shear layer, where the velocity magnitude is slightly larger than free stream.

It is evident that for the 12.5° angle of attack case, axial flow in the LEV core is not appreciably retarded at any of the x/c stations. At the most aft station, axial flow is slightly smaller, evidently attributable to a stronger influence of breakdown. Outboard of the LEV, flow is strongly retarded, with a velocity magnitude of about $0.2U_\infty$.

For the 15° AOA case, the velocity profiles are rather different. Axial flow everywhere inside the region bounded by the rolled-up LE shear layer is markedly slower than the free stream speed, with the region outboard of the LEV remnant having reversed flow. The most upstream station lacks the outboard region of reversed flow, but it also lacks a discernable local velocity peak attributable to a LEV.

In terms of the mean axial velocity profiles, it is not unreasonable to conclude that at 12.5° angle of attack, vortex breakdown occurs downstream of the domain of interrogation, but reaches the apex at 15° angle of attack. This is consistent with the flow visualizations, where the average VB location at 12.5° was at x/c ~0.5, whereas at 15°, on VB location in an averaged sense could be elucidated.

Thus, contrary to initial expectation, the leeward-side flowfield appears to vary little in going downstream in the vicinity of the wing apex.

Streamwise vorticity component

Contours of axial vorticity are given in crossflow planes for the 65° wing and 50° wing for the representative case of 15° angle of attack (Figure 13). The scope of these data is essentially identical to what one would have obtained from classical 2-D PIV. Regions of high positive and negative vorticity are generally present in all data sets. The intermediate range of near-zero vorticity is contaminated by noise, either due to the numerical noise of differentiating discrete data, or of the general amplification of errors in PIV. Whereas it is clear from the velocity vector plots that the primary LEV core will be a region of strong axial vorticity, at least in crossflow planes upstream of breakdown, small regions of concentrated vorticity ("sub-structures"), such as those observed by Shih and Ding[3], Gad-el-Haq and Blackwelder[13], and others, can not be observed from the velocity plots alone. These were, however, clearly visible in the rolling-up shear layer and in the leeward surface

boundary layer, especially where the latter is close to the primary LEV. In these plots, the data are "instantaneous."

The actual numerical values of vorticity are to be viewed with caution, since "peak" values strongly skew the entire image, and these peaks are easily affected by numerical noise and the windowing resolution of PIV. This is especially apparent at the wing leading edge region. Also, it should be mentioned that the computed sign of vorticity is the reverse of the general convention. This is strictly a consequence of sign conventions introduced by intermediate calculations.

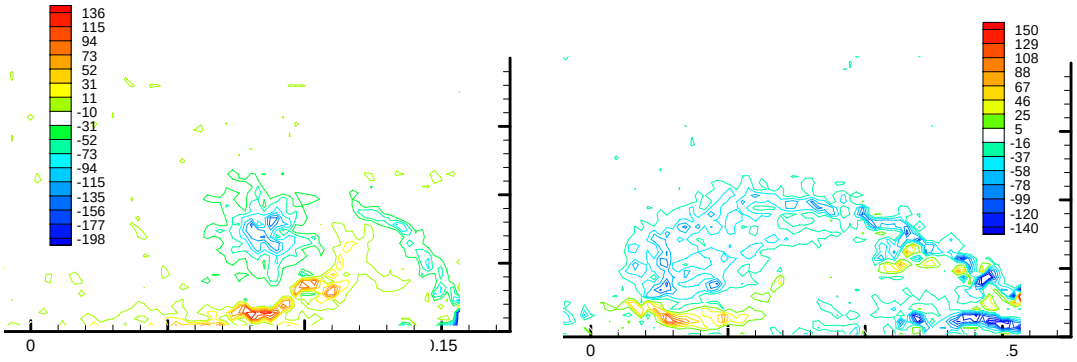

65° wing 50° wing

Figure 13. Axial vorticity contours, 65° wing and 50° wing, α = 15°

The 50° wing plot does not show an axial vorticity peak in the general vicinity of the primary LEV core. This differs from the classical pre-breakdown picture, such as that for the 65° wing for the same conditions. For both wings, a "slab" of vorticity of the opposite sense near the leeward boundary layer is also present in the region where the shear layer rollup approaches the wing leeward surface, but the phenomenon is much stronger for the 65° wing, where a coherent LEV is still present. The region between the boundary layer vorticity slab and the leading edge shear layer is largely devoid of vorticity, further supporting the assertion that this flow is essentially stagnant. Also in the 65° wing case, sub-structures of local vorticity peaks in the LEV core region, the LE shear layer and the near-surface slab are all mutually of the same sign, ruling out the presence of counter-rotating vortex pairs. But for the 50° wing, the shear layer exhibits regions of both positive and negative vorticity peaks. This has implications of the balance of vorticity production and convection over the entire flowfield of the wing[14]. If the LE shear layer contains contour-rotating structures, there is no longer the need to sustain a stable LEV as a downstream sink of vorticity, as would have been the case were the vorticity in the LE shear layer all of one sign.

Three vorticity components

SPIV is only a semi-3D technique, since the interrogation domain is still planar. In the orientation of the present setup, streamwise-direction velocity gradients can not be measured directly. In particular, this means that SPIV does not yield any more information about the vorticity than does regular planar PIV. The streamwise gradients can, however, be obtained from a crude computational scheme by arranging three SPIV interrogation planes into a closely-spaced triplet. Central differencing of the velocity data window-by-window across these adjacent SPIV interrogation planes then yields all three components of vorticity, assembling the full vorticity vector, $\vec{\omega}$. These data are only in the averaged sense, since the three SPIV interrogation planes are imaged sequentially and not simultaneously.

Such 3-plane data were taken for the 65° and 50° wings at α=15° (Figure 14). Vorticity is shown as a vector field. First, the streamwise view is given. The color bar corresponds to the total

magnitude, whence there are no negative values. Next, the planform view is shown, for which the color bar corresponds to just the out-of-plane vorticity component.

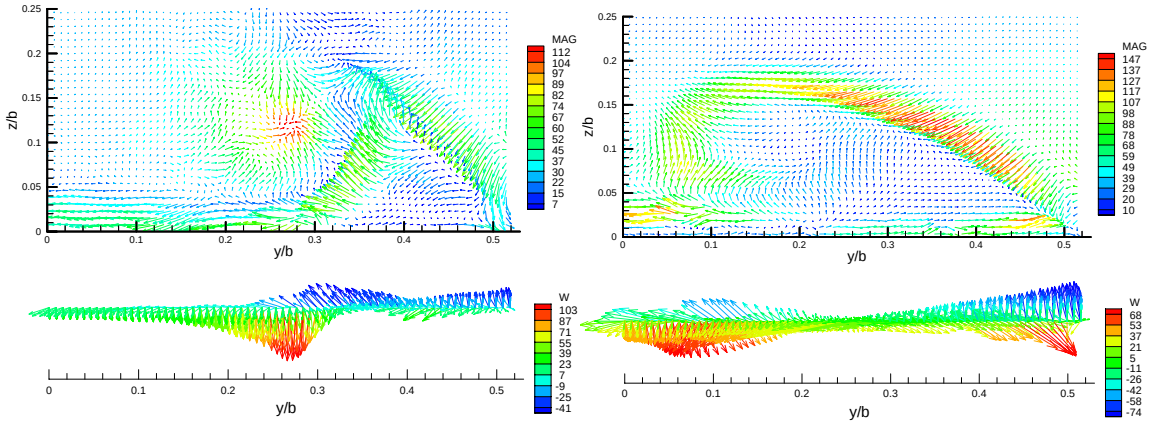

Figure 14. 65° and 50° wing, α = 15°, mean 3-component vorticity vector field, x/c = 0.296; streamwise and planform views

Here we see strong out-of-plane vorticity in the LEV core, as expected for a slender delta wing. Vorticity at the wing leeward surface inboard of the primary attachment line is indicative of that produced by a boundary layer velocity profile – and thus, of attached boundary layer flow. It should be noted that the peak value of out-of-plane vorticity component is smaller than that of the 2-D vorticity contour plots. This is for two reasons. First, the numerical method used to compute out-of-plane vorticity from planar data is less dissipative than the differencing method used for the 3-D vorticity. Second, the source of the 2-D plots is instantaneous data, while for the 3-D plots it is averaged data.

The 50° wing α=15° case exhibits appreciably less vorticity in the region bounded by the rolling-up shear layer. The planform view of the vorticity field shows that there is still a vortical structure identifiable as the primary LEV. But the vorticity in the shear layer, especially the region nearest the leading edge, is certainly dominant.

Conclusions

The slenderness of a delta wing has a more pronounced effect on the vortex flowfield as angle of attack increases. At α = 5°, the 50° and 65° exhibited remarkably similar velocity distributions over the leeward side, at least in regions far from the trailing edge. But as angle of attack was increased, the flowfield features of the two wings progressively diverged.

The 50° wing exhibits a stable separated vortical flow at angles of attack below 10°; in particular, primary LEVs are present over the entire planform at 5° and below. However, the axial velocity in the primary LEV core never exceeds the free stream velocity, even well upstream of any observable breakdown. By 20° the leeward flow is essentially stalled, with no evidence of a residual LEV. In going from the former to the latter condition, several steps were identified. The first of these is the decay of the secondary LEV, and gradual upstream progression of the primary LEV breakdown point. Then, in the 12.5°-15° range, the primary LEV breakdown is highly unsteady and sweeps over the forward half of the wing planform. By 15° the LEVs are sufficiently weakened that breakdown-like state appears to cover the entire planform. Finally, by 20°, flow inboard of the primary LEVs is itself stalled, yet an organized leading edge shear layer rollup is still observed. At the Reynolds numbers considered in this investigation, flow outboard of the primary LEV is unexpectedly weak, while the region of the velocity profiles normally associated with the primary LEV is quite broad.

In further work, it would be interesting to extend the SPIV results to the 65° wing at higher angles of attack, and to consider the trailing edge region and the near wake of both wings. Also, since the 50° wing exhibits definite leading edge vortices, wings of yet lower sweep should be tested to ascertain a more extreme bound for sweep where coherent leading edge vortical flow is no longer possible. Finally, more work needs to be done to ascertain the parametric dependency of the flow field on Reynolds number, especially if results from low-Re experimental data are to be associated with high-Re applications.

The abruptness of the stall of the 50° wing, the large-scale unsteadiness en route to stall and the presence of a coherent leading edge shear layer long after LEV breakdown are qualitatively indicative of a transitional case from slender delta wing separation to classical airfoil stall.

References

[1] Kuechemann, D. The Aerodynamic Design of Aircraft. 1976.

[2] Ayoub, A., and McLachlan, B.G. "Slender Delta Wing at High Angles of Attack – a Flow Visualization Study". AIAA paper # 87-1230, June 1987.

[3] Shih, C., and Ding, Z. "Unsteady Structure of Leading-Edge Vortex Flow over a Delta Wing". AIAA paper # 96-0664, January 1996.

[4] Erickson, G.E. "Water Tunnel Studies of Leading-Edge Vortices." *J. Aircraft*, Vol. 19, No. 6, pp. 442-448. 1981.

[5] Poisson-Quinton, P. and Werle, H. "Water-Tunnel Visualization of Vortex Flow." *Aeronautics and Astronautics*, June 1967, pp. 64-66.

[6] Thompson, D.H. "A Water Tunnel Study of Vortex Breakdown over Delta Wings with Highly Swept Leading Edges." *Aerodynamics Note* 356, A.R.L. (Australia), May 1975.

[7] Miau, J.J., Kuo, K.T., Liu, W.H., Hsieh, S.J., Chou, J.H., and Lin, C.K. "Flow Developments above 50-Deg Sweep Delta Wings with Different Leading-Edge Profiles". *J. Aircraft*, Vol. 32, No. 4, Jul-Aug 1995.

[8] Earnshaw, P.B., and Lawford, J.A. "Low-Speed Wind Tunnel Experiments on a Series of Sharp-Edged Delta Wings". *Reports and Memorabilia*, No. 3424, March 1964.

[9] Ol, M. "The Passage Toward Stall of Nonslender Delta Wings and Low Reynolds Number." Ph.D. thesis, Caltech, 2001.

[10] Willert, C.E. "Stereoscopic Digital Particle Image Velocimetry for Application in Wind Tunnel Flows". *Meas. Sci. Technol.*, Vol. 8, 1997, pp. 1465-1479.

[11] Truneva, E.A. "On the Mechanism of Vortex Breakdown Point Stabilization for a Low-Subsonic Flow about a Delta Wing." Bulletin of Institutes of Higher Education, Aviation Tech. (USSR), Vol. 19, No. 2, 1976.

[12] Traub, L. "Low-Reynolds-Number Effects on Delta Wing Aerodynamics." J. Aircraft, Vol. 35, No. 4, 1998, pp. 653-656.

[13] Gad-el-Haq, M. and Blackwelder, R. F. "The Discrete Vortices from a Delta Wing." *AIAA Journal*. Vol. 23, No. 6, June 1985, pp. 961-962.

[14] Lee, M. and Ho, C.-M., "Lift Force of Delta Wings." ASME; *Appl. Mech. Rev*. Vol 43, No 9, September 1990, pp. 209-221.

Paper: #2
Author: Dr. Ol

Question by Dr. Luckring: First let me comment that Smith's similarity parameter "a" would be a better correlation parameter to use than $\propto$, especially since you are comparing two delta wings of different sweep. My question is whether you have calibrated your facility for predicting vortex breakdown locations against established data sets, such as due to Dr. Hummel or Prof. Wentz?

Answer: No, no such calibration has been done.